ELSEVIER

Journal of Crystal Growth 179 (1997) 97–107

JOURNAL OF CRYSTAL GROWTH

B incorporation and hole transport in fully strained heteroepitaxial $Si_{1-x}Ge_x$ grown on Si(0 0 1) by gas-source MBE from Si_2H_6, Ge_2H_6, and B_2H_6

Q. Lu, M.R. Sardela, N. Taylor, G. Glass, T.R. Bramblett, T. Spila, J.R. Abelson, J.E. Greene*

Department of Materials Science, The Coordinated Science Laboratory, and the Materials Research Laboratory, University of Illinois, 1101 West Springfield, Urbana, Illinois 61801, USA

Received 16 September 1996; accepted 14 January 1997

Abstract

B-doped $Si_{0.95}Ge_{0.05}$(0 0 1) films were grown on Si(0 0 1) by gas-source molecular beam epitaxy in the surface-reaction-limited regime using Si_2H_6, Ge_2H_6, and B_2H_6. Incorporated B concentrations C_B ($5 \times 10^{16} - 3 \times 10^{19}$ cm^{-3}) were found to increase linearly with increasing B_2H_6 flux $J_{B_2H_6}$ (6×10^{12}–2×10^{15} cm^{-2} s^{-1}) at constant film growth temperature T_s, and to decrease exponentially with $1/T_s$ at constant $J_{B_2H_6}$. The B_2H_6 reactive sticking probability ranged from $\simeq 3.3 \times 10^{-4}$ at $T_s = 600°C$ to 8.2×10^{-4} at 700°C and film growth rates were independent of $J_{B_2H_6}$. Structural analysis by in-situ reflection high-energy electron diffraction combined with post-deposition high-resolution plan-view and cross-sectional transmission electron microscopy, high-resolution X-ray diffraction, and reciprocal lattice mapping showed that all films were fully strained, with measured relaxations less than the detection limit, $\simeq 3 \times 10^{-5}$, and exhibited no evidence of dislocations or other extended defects. Room-temperature $Si_{0.95}Ge_{0.05}$: B conductivity mobilities were equal to theoretical values and a factor of $\simeq 2$ higher than corresponding results for bulk Si. μ_c varied from 410 cm^2 V^{-1} s^{-1} with $C_B = 5 \times 10^{16}$ cm^{-3} to 60 cm^2 V^{-1} s^{-1} with $C_B = 3 \times 10^{19}$ cm^{-3}.

PACS: 73.61; 73.80.Cj; 81.10.Aj; 61.72.T

Keywords: SiGe; B incorporation; Electronic properties; Hole mobilities; Strain

1. Introduction

The use of Si_2H_6 and/or Ge_2H_6 as precursors during gas-source molecular-beam epitaxy (GS-MBE) of Si [1], Ge [2], and $Si_{1-x}Ge_x$ [3], on Si(0 0 1) has been shown recently to provide reactive sticking probabilities of up to two orders of magnitude higher than those of SiH_4 and GeH_4, primarily due to the ease of cleaving IV–IV bonds, compared to IV–H bonds, in surface-adsorbed species. GS-MBE Si [1] and Ge [2] deposition rates

* Corresponding author. Fax: + 1 217 244 1631; e-mail:jegreene@uiuc.edu.

0022-0248/97/$17.00 Copyright © 1997 Elsevier Science B.V. All rights reserved
PII S0022-0248(97)00116-4

R as functions of incident fluxes $J_{Si_2H_6}$ and $J_{Ge_2H_6}$ and growth temperature T_s (300–950°C) are well-described in both the high-temperature flux-limited and low-temperature surface-reaction-limited regimes by a model based upon dissociative chemisorption of the dimeric hydride species followed by a series of surface decomposition reactions with the rate-limiting step being first-order hydrogen desorption from Si or Ge monohydride. The zero-coverage Si_2H_6 reactive sticking probability $S^{Si}_{Si_2H_6}$ on Si(0 0 1) was determined from R_{Si} versus $J_{Si_2H_6}$ data to be 0.036 [1], essentially independent of temperature, in the flux-limited regime while the activation energy for first-order H_2 desorption from Si monohydride was $E_{Si\text{-}H}$ = 2.04 eV [1, 4]. In the case of Ge_2H_6, $S^{Ge}_{Ge_2H_6}$ was found to be 0.056 with $E_{Ge\text{-}H}$ = 1.56 eV [2]. B reactive sticking probabilities in GS-MBE Si(0 0 1) layers grown from Si_2H_6 and B_2H_6 ranged from $\simeq 6.4 \times 10^{-4}$ at $T_s = 600$°C to 1.4×10^{-3} at 950°C and temperature-dependent hole carrier mobilities were equal to the best reported bulk Si : B values [5].

In this article, we report the results of an investigation of B incorporation in fully strained $Si_{0.95}Ge_{0.05}$ alloys grown on Si(0 0 1) by GS-MBE from Si_2H_6, Ge_2H_6, and B_2H_6. A relatively dilute alloy composition was chosen for these experiments and deposition was carried out in the surface-reaction-limited growth regime near the upper temperature range, 600–700°C, in order to minimize film composition changes as a function of T_s. At lower growth temperatures where the steady-state hydrogen surface concentration becomes appreciable, the Ge alloy fraction increases with decreasing T_s – for constant Si_2H_6 and Ge_2H_6 fluxes – due to a combination of the lower activation energy for hydrogen desorption from Ge than from Si and the higher reactive sticking probability of Ge_2H_6, compared to Si_2H_6, on Ge.

The $Si_{0.95}Ge_{0.05}$ films, with thicknesses ranging from 300 to 800 nm, were found by high-resolution X-ray diffraction reciprocal lattice-mapping to be fully strained. B-doping profiles, measured by secondary ion mass spectrometry, were abrupt to within the experimental resolution, 8 nm per concentration decade. B_2H_6 reactive sticking probabilities ranged from $\simeq 3.3 \times 10^{-4}$ at $T_s = 600$°C to 8.2×10^{-4} at 700°C and the film growth rates were independent of $J_{B_2H_6}$ over the range investigated, 6×10^{12}–2×10^{15} cm^{-2} s^{-1}, corresponding to incorporated B concentrations $C_B = 5 \times 10^{16}$–3×10^{19} cm^{-3}. Room-temperature conductivity mobilities varied from 410 cm^2 V^{-1}s^{-1} with $C_B = 5 \times 10^{16}$ cm^{-3} to 60 cm^2 V^{-1}s^{-1} with $C_B = 3 \times 10^{19}$ cm^{-3} in good agreement with Boltzmann transport model calculations [6] accounting for changes in the valence-band structure due to the effects of both alloying and biaxial in-plane compressive strain.

2. Experimental procedure

All films were grown in a multi-chamber ultra-high-vacuum system, described in more detail in Refs. [2, 5], which was evacuated using a combination of ion and turbomolecular pumps to provide a base pressure of $\simeq 1 \times 10^{-10}$ Torr. The film growth chamber, equipped with an in-situ reflection high-energy electron diffraction (RHEED) apparatus and a quadrupole mass spectrometer, is connected through the transfer chamber to an analytical station containing provisions for Auger electron spectroscopy (AES), electron energy loss spectroscopy, low-energy electron diffraction, and temperature-programmed desorption. The final chamber contains a scanning tunneling microscope.

During film deposition, Si_2H_6, Ge_2H_6, and B_2H_6 molecular beams are delivered to the substrate through individual directed tubular dosers located 3 cm from the substrate at an angle of 45°. The dosers are coupled to feedback-controlled constant-pressure reservoirs in which pressures are separately monitored using capacitance manometers whose signals are in turn used to control variable leak valves. Valve sequencing, pressures, gas flows, and substrate temperature are all controlled through a computer.

More than 50 B-doped single-layers, 300–800 nm thick, and multilayer modulation-doped films were grown for these experiments. For the single-layer films, Si_2H_6, Ge_2H_6, and B_2H_6 beams were simultaneously incident at the substrate during film growth. In the case of the modulation-doped samples, however, sequential doped layers within

a single alloy film were separated by undoped spacer layers.

The Si(0 0 1) substrates were $1 \times 3\,cm^2$ plates cleaved from 0.5 mm thick n-type (resistivity = 23–28 Ωcm, $n = 1–2 \times 10^{14}\,cm^{-3}$) wafers. Initial cleaning consisted of degreasing by successive rinses in trichloroethane, acetone, propanol, and distilled water. The substrates were then subjected to four wet-chemical oxidation/etch cycles consisting of the following steps: 2 min in a 6 : 1 : 1 solution of $H_2O : HCl : H_2O_2$, rinse in fresh deionized water, and a 20 s etch in dilute (10%) HF. The substrates were blown dry in dry N_2, exposed to a UV/ozone treatment which consists of UV irradiation from a low-pressure Hg lamp ($15\,mW\,cm^{-2}$) for 30 min in air to remove C-containing species [7], and introduced into the deposition system through the transfer chamber where they were degassed at 250°C for 3 h and then rapidly heated at $\simeq 20°C\,s^{-1}$ to 1100°C for 2 min to remove the oxide. RHEED patterns from substrates subjected to this procedure were 2×1 with sharp Kikuchi lines. No residual C or O was detected by AES.

Deposited film thicknesses were measured using microstylus profilometry and Rutherford backscattering (RBS), while alloy compositions were determined by RBS. The RBS probe beam consisted of 2 MeV He^+ ions incident at 15° to the sample surface with the detector set at a 150° scattering angle. Backscattering spectra were analyzed using the RUMP simulation program [8], and the reported film compositions are accurate to within 1 at%. B concentrations in as-deposited layers were determined using a Cameca IMS-5F secondary ion mass spectrometer (SIMS) operated with a 10 keV O_2^+ primary ion beam to detect ^{11}B. Quantification was carried out by comparison to B ion-implanted bulk $Si_{1-x}Ge_x$ standards yielding an experimental uncertainty of ± 10%. Other than intentionally introduced B, the films contained no detectable impurities.

High-resolution X-ray diffraction (HR-XRD) measurements were performed using a four-axis diffractometer with a Bartels four-crystal Ge monochromator and an Euler sample cradle with independent computer-controlled drive of all sample rotation angles. The instrument is capable of positioning samples to within 0.00025°. Cu-K_α radiation with an angular divergence < 12 arcsec and a wavelength spread of $\simeq 2 \times 10^{-5}$ was incident at an angle ω with respect to the sample surface. Overview ω–2θ scans, where θ is the diffraction angle, were performed using a wide-aperture ($\simeq 2°$) detector with a rotation rate twice that of the sample. In order to investigate the orientation dependence of X-ray scattering distributions from the films, the detector acceptance was reduced to 7–12 arcsec by placing a two-reflection Ge crystal analyzer between the sample and the detector. High-resolution reciprocal space maps were then constructed by carrying out successive ω–2θ scans, centered at different values of ω, in the triple-axis mode. Recorded intensities are plotted in a two-dimensional contour map as a function of reciprocal space wave vectors k parallel and perpendicular to the surface.

Plan-view and cross-sectional transmission electron microscopy (TEM and XTEM) examinations were carried out in Phillips CM120 and EM420 microscopes operated at 120 kV while high-resolution lattice images were obtained at 300 kV using a Hitachi H9000 microscope. Sample preparation for TEM and XTEM investigations followed the procedure described in Refs. [3, 5].

Resistivity and Hall-effect measurements were conducted at room-temperature using the van der Pauw technique [9]. Ohmic contacts were formed by evaporating Al through a mask and rapid-thermal annealing the sample at 300°C for 10 s. In-clad Pt electrical leads were then soldered to the Al contacts. The magnetic field strength for the Hall measurements was 10 kG.

3. Experimental results and discussion

3.1. Film growth kinetics

Fig. 1 shows measured deposition rates R_{SiGe} as a function of T_s for GS-MBE $Si_{0.95}Ge_{0.05}$ films grown with $J_{Si_2H_6} = 4.7 \times 10^{16}\,cm^{-2}\,s^{-1}$ and $J_{Ge_2H_6} = 2.7 \times 10^{14}\,cm^{-2}\,s^{-1}$. For comparison, results are also presented for the growth of pure Si using the same Si_2H_6 flux, $J_{Si_2H_6} = 4.7 \times 10^{16}\,cm^{-2}\,s^{-1}$. In both the cases, GS-MBE

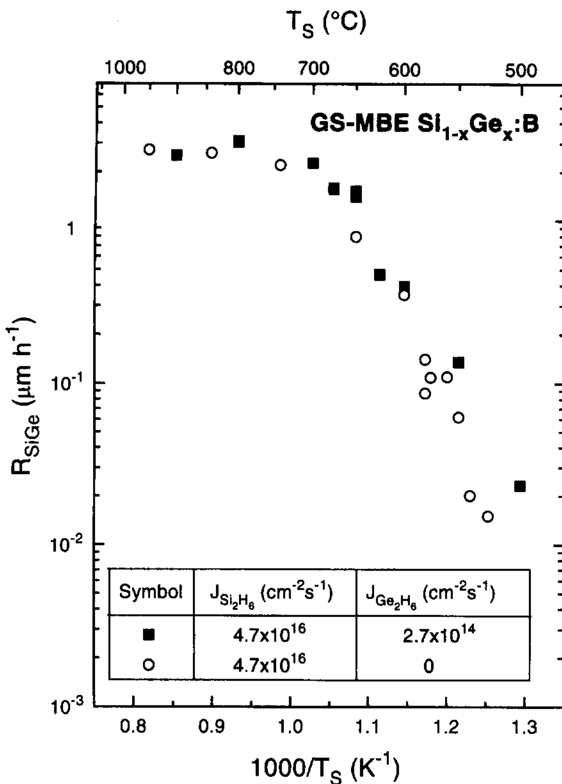

Fig. 1. Growth rates R_{Si} and R_{SiGe} of Si and $Si_{0.95}Ge_{0.05}$ films deposited on Si(0 0 1)2 × 1 by GS-MBE as a function of temperature T_s. The incident Si_2H_6 and Ge_2H_6 fluxes, $J_{Si_2H_6}$ and $J_{Ge_2H_6}$, were 4.7×10^{16} and 2.7×10^{14} cm^{-2} s^{-1}, respectively.

deposition rates R as a function of T_s follow the general form expected for chemical vapor deposition (CVD) in which R saturates at high temperatures in an impingement-flux-limited growth mode while at low temperatures, R decreases exponentially with $1/T_s$ indicative of surface-reaction-limited growth. The addition of the relatively small Ge_2H_6 flux has, as expected, only a minor effect on film deposition rates at elevated temperatures. However, in the lower-temperature surface-reaction-limited regime, where R is limited by hydrogen desorption, the deposition rate of the alloy is higher than that of Si primarily due to the lower activation energy for hydrogen desorption from Ge [2] than from Si [1, 4]. Similar results have been reported previously for $Si_{1-x}Ge_x$ growth by both CVD and GS-MBE from SiH_4 and GeH_4 monomer source gases [11–14].

Over the growth temperature range of the $Si_{0.95}Ge_{0.05}$ B-doping experiments, R_{SiGe} increases from 0.4 μm h^{-1} at $T_s = 600$°C to 2.3 μm h^{-1} at 700°C. The use of a concurrent B_2H_6 flux during film growth was found to have no measurable effect on deposition rates over the entire flux range investigated: $J_{B_2H_6} = 6 \times 10^{12}$–$2 \times 10^{15}$ cm^{-2} s^{-1}.

3.2. Film microstructure and strain state

A combination of HR-XRD, TEM, and XTEM was employed to examine the microstructure, crystalline quality, and the degree of relaxation in the GS-MBE $Si_{0.95}Ge_{0.05}$(0 0 1) alloys. HR-XRD is much more sensitive than TEM to the initial stages of film relaxation through misfit dislocation generation. The resolution for detecting changes in film/substrate lattice-constant misfit in the present HR-XRD measurements is $\simeq 2 \times 10^{-5}$ corresponding to a linear dislocation density of 1×10^3 cm^{-1} or an average dislocation separation of $\simeq 10$ μm.

All films were found to be fully strained. Fig. 2a shows a typical overview 004 ω–2θ scan, obtained

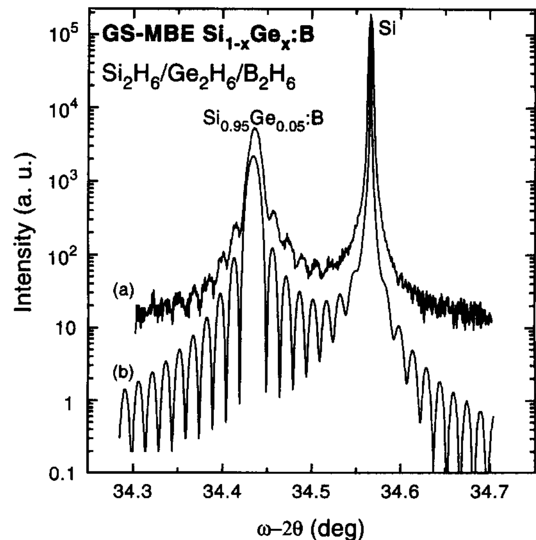

Fig. 2. (a) High-resolution X-ray-diffraction 004 ω–2θ scan from a GS-MBE $Si_{0.95}Ge_{0.05}$ layer grown on Si(0 0 1) at $T_s = 650$°C. (b) Fully dynamical simulation, assuming no strain relaxation with uniform flat lattice planes and a perfectly abrupt film/substrate interface.

with an open detector, from a $Si_{0.95}Ge_{0.05}$/Si(0 0 1) structure grown at 650°C with an alloy layer thickness of 360 nm. A sharp film peak with full-width at half-maximum (FWHM) intensity $\Gamma_{\omega-2\theta} = 40$ arcsec is obtained at $-0.131°$ (-470 arcsec) on the low-angle side of the substrate peak for which $\Gamma_{\omega-2\theta} = 15$ arcsec. An indication of the high structural quality of the alloy film is the presence of the finite-thickness fringes in Fig. 2a which arise due to interference of diffracted waves scattered from a finite number of lattice planes. The presence of the fringes indicates that the lattice planes are uniform and flat [15].

A simulated 004 rocking curve, based upon the fully dynamical formalism developed by Taupin [16] and Takagi [17], is shown in Fig. 2b for comparison. The simulation was carried out assuming a perfectly abrupt and coherent film/substrate interface. The measured and simulated curves are in very good agreement with respect to the angular positions and relative intensities of not only the primary diffraction peaks, but also the thickness fringes. Similar good agreements were obtained for all the samples analyzed.

More detailed analyses were carried out using high-resolution reciprocal lattice mapping. Fig. 3 shows a typical lattice map around the 1 1 3 reflection for the same sample used to obtain the rocking curve data in Fig. 2. Diffracted intensity distributions are plotted as isointensity contours as a function of the reciprocal space wave vectors parallel and perpendicular to the sample surface, $k_{\parallel}$ and $k_{\perp}$. The fact that the centers of the substrate and film scattering distributions are aligned in the $k_{\parallel}$ direction indicates negligible in-plane strain relaxation, i.e. fully commensurate growth. From high precision measurements of $k_{\parallel}$ for the film and substrate, the degree of strain relaxation was found to be $(3 \pm 3) \times 10^{-5}$, within the detection limit of the instrument. Thus, the in-plane lattice parameter of the film, $a_{\parallel,SiGe} = 0.54312 \pm 0.00002$ nm, is essentially equal to that of the substrate, $a_{Si} = 0.54310$ nm. The vertical separation between the film and substrate diffracted intensity distributions in Fig. 3 corresponds to a tetragonal lattice constant mismatch in the growth direction of $(3.28 \pm 0.03) \times 10^{-3}$ yielding $a_{\perp,SiGe} = 0.54488 \pm 0.00002$ nm.

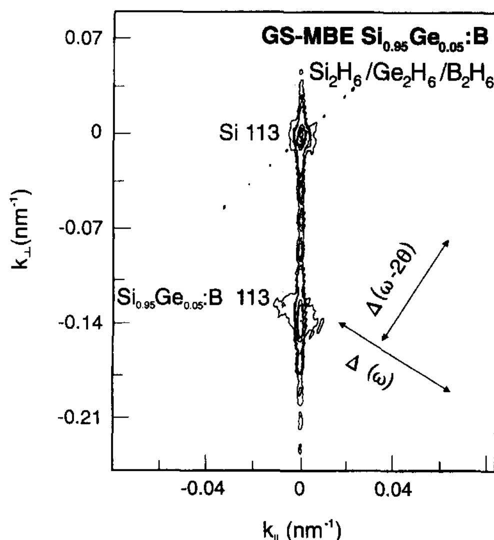

Fig. 3. Triple-axis high-resolution 113 reciprocal-space map from the $Si_{0.95}Ge_{0.05}$ alloy corresponding to Fig. 2. Successive isointensity contours are 42500, 21250, 4250, 1010, 505, 50.5, 30 and 10 counts s^{-1}.

The film diffraction contours in Fig. 3 are nearly symmetric with no distortions except for elongations along the growth direction due to crystal truncation (finite thickness) effects. Elongation of the diffraction contours in the in-plane, ω, or ω–2θ directions would signify the presence of nanocrystalline phases, misfit dislocations, or significant strain variations [18]. The FWHM values measured along these directions in Fig. 3 are: $\Gamma_{\parallel} = 8$ arcsec, $\Gamma_{\omega} = 13$ arcsec, and $\Gamma_{\omega-2\theta} = 14$ arcsec. These values are comparable to the corresponding values for the substrate diffraction distribution. In addition, the square root of the sum of the squares of these values is essentially equal to the minimum theoretical total FWHM value for this alloy, 21 arcsec, calculated based upon the intrinsic peak width $\simeq 6$ arcsec [19], while accounting for strain broadening due to the lattice-constant mismatch and finite thickness effects [20]. Thickness fringes are also observed in Fig. 3 as diffracted intensity distributions positioned periodically along the film growth direction. The diffraction distribution line passing transversely through the substrate peak is due to residual scattering from the analyzer crystal.

The presence of B in these alloy films partially compensated the compressive strain due to Ge

alloying. This was easily detectable in XRD scattering distributions at high B concentrations. $C_B = 2 \times 10^{19}$ and 3×10^{19} cm^{-3} correspond to alloy 0 0 4 peak shifts with respect to Si of $\simeq 38$ and 54 arcsec, respectively.

Plan-view 0 0 4 bright-field micrographs of these films are featureless with no indication of interfacial misfit dislocations. Selected-area electron diffraction patterns obtained near the [0 0 1] zone axis consist of single-crystal reflections with symmetric intensities. $\bar{1}10$ XTEM and HR-XTEM images also revealed the films to be highly perfect with no visible extended defects or residual damage. The 1 1 1 lattice fringes are continuous across the film/substrate interface with no indication of disorder.

3.3. B incorporation

A typical SIMS depth profile through a B modulation-doped $Si_{0.95}Ge_{0.05}$(0 0 1) film grown at $T_s = 650°C$ with successive 400 nm thick doped layers separated by 200 nm thick undoped buffer layers is shown in Fig. 4. The B_2H_6 fluxes used to obtain the doped regions were 5.5×10^{13}, 1.8×10^{14}, and 3.0×10^{14} cm^{-2} s^{-1} resulting in steady-state B concentrations C_B of 8.2×10^{17}, 2.8×10^{18}, and 4.8×10^{18} cm^{-3}, respectively. All SIMS profiles obtained from B modulation-doped samples had leading and trailing edges which were abrupt to within the experimental resolution, 8 nm per concentration decade. No tendency for B surface segregation was observed in either modulation-doped or single-layer films.

The variations in C_B as a function of $J_{B_2H_6}$ and T_s were determined from quantitative SIMS analyses of modulation-doped samples, such as the one shown in Fig. 4, and B-doped single-layer films. Fig. 5 shows that at a constant film growth temperature, C_B increases linearly with increasing $J_{B_2H_6}$. With a constant B_2H_6 flux, $\ln(C_B)$ decreases with increasing $1/T_s$. Temperature-dependent data are shown in Fig. 6 for $Si_{0.95}Ge_{0.05}$ films grown with dopant fluxes $J_{B_2H_6}$ of 5.4×10^{13}, 2.9×10^{14}, 4.9×10^{14}, and 8.1×10^{14} cm^{-2} s^{-1} corresponding to $J_{B_2H_6}/(J_{Si_2H_6} + J_{Ge_2H_6})$ flux ratios ranging from 1.1×10^{-3} to 1.7×10^{-2}.

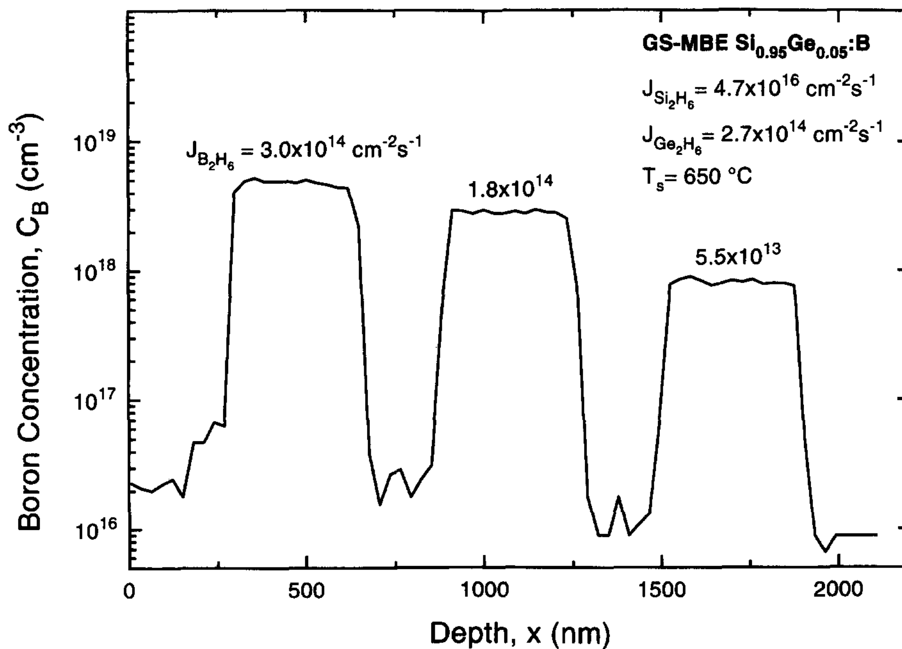

Fig. 4. SIMS depth profiles through a B modulation-doped $Si_{0.95}Ge_{0.05}$(0 0 1) film grown by GS-MBE at 650°C. The incident Si_2H_6 and Ge_2H_6 fluxes, $J_{Si_2H_6}$ and $J_{Ge_2H_6}$, were 4.7×10^{16} and 2.7×10^{14} cm^{-2} s^{-1}, respectively, while the B_2H_6 flux, $J_{B_2H_6}$, was varied from 5.5×10^{13} to 3.0×10^{14} cm^{-2} s^{-1}.

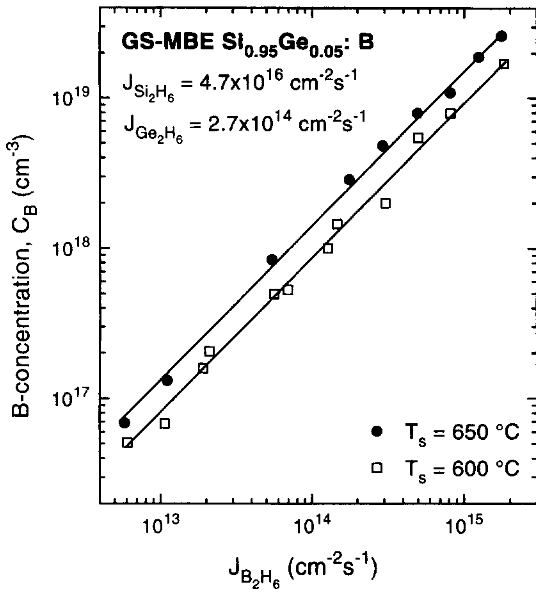

Fig. 5. B dopant concentration C_B incorporated in GS-MBE $Si_{0.95}Ge_{0.05}$(0 0 1) films grown at T_s = 600–650°C as a function of the incident B_2H_6 flux, $J_{B_2H_6}$, with $J_{Si_2H_6}$ and $J_{Ge_2H_6}$ maintained constant at 4.7×10^{16} and 2.7×10^{14} cm^{-2} s^{-1}, respectively.

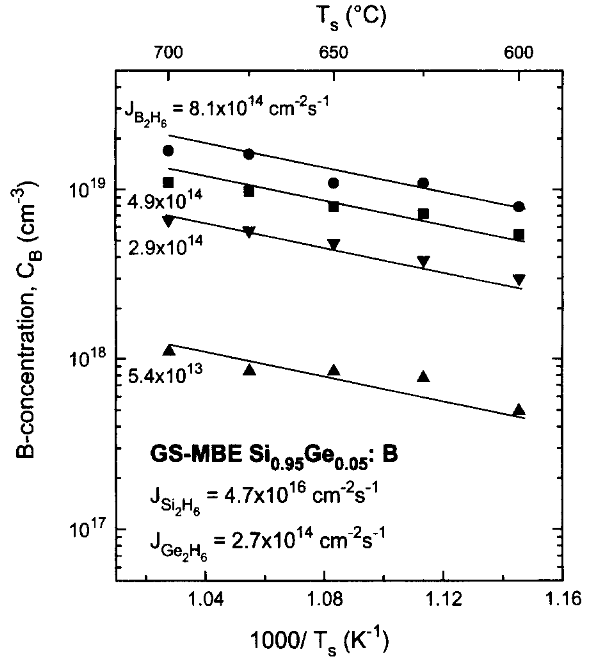

Fig. 6. B dopant concentration C_B incorporated in GS-MBE $Si_{0.95}Ge_{0.05}$(0 0 1) films as a function of film growth temperature T_s for B_2H_6 fluxes $J_{B_2H_6}$ between 5.4×10^{13} and 8.1×10^{14} cm^{-2} s^{-1} with $J_{Si_2H_6}$ and $J_{Ge_2H_6}$ maintained constant at 4.7×10^{16} and 2.7×10^{14} cm^{-2} s^{-1}, respectively.

B_2H_6 is known to dissociatively adsorb on Si(0 0 1) with a saturation coverage which is reduced by the presence of surface hydrogen [21]. Thus, as is the case for Si_2H_6 [1] and Ge_2H_6 [2], the primary B_2H_6 adsorption path during GS-MBE $Si_{0.95}Ge_{0.05}$ deposition is through reaction with surface dangling bonds. Consequently, the B deposition rate should be expressible by an equation analogous to those derived in Refs. [1, 2] to describe GS-MBE Si and Ge growth rates,

$$R_B = \frac{2 J_{B_2H_6} S_{B_2H_6} \theta_{db}^x}{N_{SiGe}}, \tag{1}$$

where $S_{B_2H_6}$ is the zero-coverage B_2H_6 reactive sticking probability, x is the kinetic order of the B_2H_6 adsorption reaction with respect to dangling-bond coverage θ_{db}, and N_{SiGe} is the $Si_{0.95}Ge_{0.05}$ atom number density. In the limit of very dilute B surface concentrations, which is the case in these experiments where the ratio $J_{B_2H_6}/(J_{Si_2H_6} + J_{Ge_2H_6})$ is small and there is no measurable B surface segregation, the incorporated B doping concentration C_B is given by

$$C_B = \frac{J_{B_2H_6} S_{B_2H_6} \theta_{db}^x}{(J_{Si_2H_6} S_{Si_2H_6} + J_{Ge_2H_6} S_{Ge_2H_6}) \theta_{db}^2} N_{SiGe}, \tag{2}$$

in which $S_{Si_2H_6}$ and $S_{Si_2H_6}$ are the reactive sticking probabilities of Si_2H_6 and Ge_2H_6.

Si and Ge SIMS profiles from the B-doped $Si_{0.95}Ge_{0.05}$ samples used in these experiments, as well as from $Si_{0.95}Ge_{0.05}$/Si superlattices, exhibit no detectable Ge segregation. Given the large difference between Si_2H_6 and Ge_2H_6 reactive sticking probabilities on Si [1, 2, 10], this is consistent with the results in Fig. 1 showing that the temperature-dependent growth rates of $Si_{0.95}Ge_{0.05}$ and Si are nearly equal at T_s = 600–700°C. Moreover, the reactive sticking probabilities of Si_2H_6 and Ge_2H_6 are almost an order of magnitude larger on Si than on Ge [1, 2, 10]. Thus, the terms $S_{Si_2H_6}$ and $S_{Ge_2H_6}$ in Eq. (2) can be approximated by the values of the reactive sticking probabilities of Si_2H_6 and Ge_2H_6

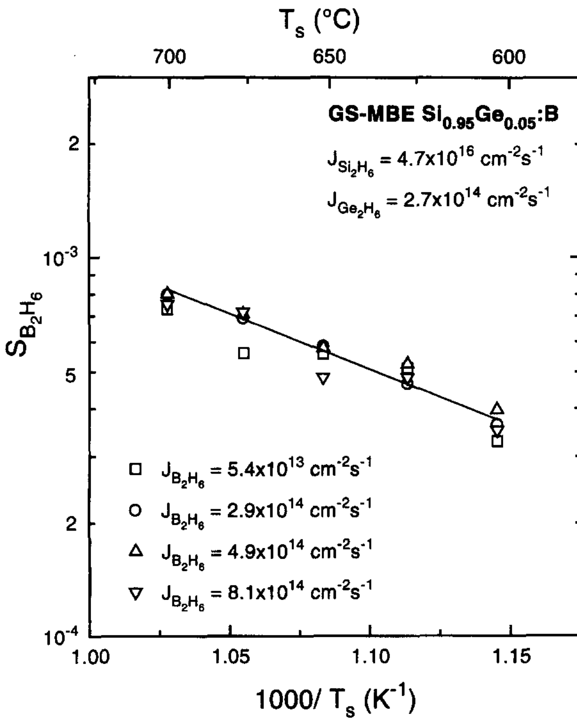

Fig. 7. The B_2H_6 reactive sticking probability $S_{B_2H_6}$ as a function of temperature T_s during the growth of B-doped GS-MBE $Si_{0.95}Ge_{0.05}(0\,0\,1)$ films. The Si_2H_6 and Ge_2H_6 fluxes were maintained constant at 4.7×10^{16} and 2.7×10^{14} cm^{-2} s^{-1}, respectively, while the B_2H_6 flux was varied between 5.4×10^{13} and 8.1×10^{14} cm^{-2} s^{-1}.

on Si. The error introduced by this approximation is less than the experimental uncertainty in measuring C_B, $\pm 10\%$. From previous growth kinetics studies, $S^{Si}_{Si_2H_6} = 0.036$ [1] and $S^{Si}_{Ge_2H_6} = 0.33$ [10] with very little temperature dependence over the T_s range of these experiments.

Fig. 6 shows that $\ln(C_B)$ decreases linearly with increasing $1/T_s$ for all $J_{B_2H_6}$ values investigated, 5.4×10^{13}–8.1×10^{14} cm^{-2} s^{-1}. Considering the complex T_s dependence associated with the term θ_{db} [1, 2] in Eq. (2), the experimental results indicate that the kinetic order of the B_2H_6 adsorption reaction is the same as that of Si_2H_6 and Ge_2H_6, and hence is assumed to be 2. Setting $x = 2$ in Eq. (2), the temperature dependence of C_B for a constant incident flux ratio is determined by the term $J_{B_2H_6}S_{B_2H_6}/(J_{Si_2H_6}S_{Si_2H_6} + J_{Ge_2H_6}S_{Ge_2H_6})$. All the data in Fig. 5, irrespective of $J_{B_2H_6}$, are replotted in Fig. 7, using Eq. (2) and the $S_{Si_2H_6}$ and $S_{Ge_2H_6}$ values given above, as $S_{B_2H_6}$ versus $1/T_s$ and fitted using a least-squares analysis. The sign of the slope indicates that, contrary to Si_2H_6 and Ge_2H_6 for which chemisorption is precursor mediated [1, 2], the chemisorption of B_2H_6 on $Si_{0.95}Ge_{0.05}$ is thermally activated in agreement with the previous results for B_2H_6 on Si [5]. Values for $S_{B_2H_6}$ in Fig. 7 range from $\simeq 3.3 \times 10^{-4}$ at $T_s = 600$°C to 8.2×10^{-4} at 700°C, a little lower than the values previously reported for B_2H_6 on pure Si(0 0 1) [5] with a somewhat stronger T_s-dependence. Eq. (2) also shows that at constant T_s, $C_B \propto J_{B_2H_6}/(J_{Si_2H_6} + J_{Ge_2H_6})$ in agreement with the results in Fig. 5.

3.4. Transport properties

The hole conductivity mobility μ_c of fully strained B-doped GS-MBE $Si_{0.95}Ge_{0.05}(0\,0\,1)$ alloys was determined using B concentrations obtained from SIMS and resistivities ρ from van der Pauw [9] measurements. We have assumed that B acceptor concentrations are equal to C_B, i.e. that all dopant atoms are electrically active. We know this to be the case for B-doped GS-MBE Si where N_a was obtained independently from fitting $\rho(T)$ data with the charge neutrality equation [5] including the B acceptor ionization energy in Si, $E_B = 45$ meV [22]. Unfortunately, E_B as a function of x in $Si_{1-x}Ge_x$ is unknown. However, the good agreement between our measured and calculated $Si_{1-x}Ge_x$ mobilities presented below provides indirect evidence that the assumption of complete electrical activity is reasonable. In addition, while it has been shown that the B acceptor ionization probability decreases slowly with increasing Ge concentration in $Si_{1-x}Ge_x$ alloys due to a corresponding decrease in the valence-band density of states [23], absolute ionization probabilities are not known. Thus, we have simply taken the hole carrier concentration p as being equal to C_B which introduces an error estimated to be $\leqslant 10\%$ and within the experimental uncertainty in measured values of C_B. The mobility was then determined from the relationship $\mu_c = 1/(q\ \rho\ p)$ where q is the elementary charge.

Fig. 8 shows room-temperature conductivity mobilities for GS-MBE $Si_{0.95}Ge_{0.05}$ alloys as

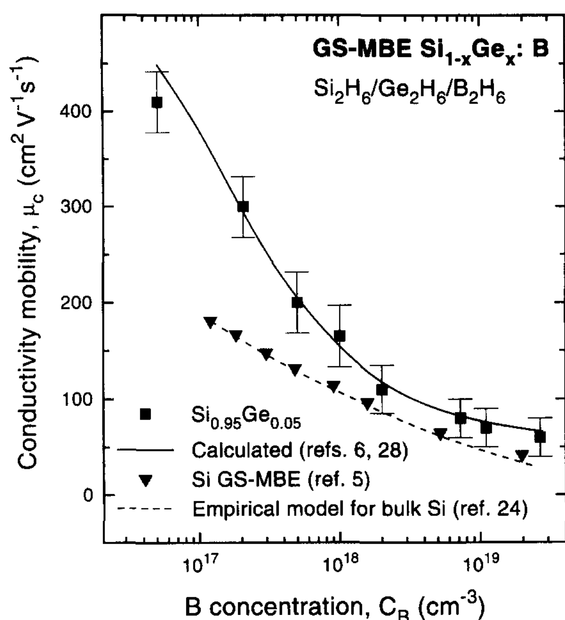

Fig. 8. Room-temperature hole conductivity mobilities μ_c as a function of the carrier concentration C_B in fully strained GS-MBE $Si_{0.95}Ge_{0.05}$ films grown on Si(0 0 1) at T_s = 550–600°C. Data from B-doped GS-MBE Si(0 0 1) layers grown at T_s = 700°C (Ref. [5]) and bulk Si : B (Ref. [24]) are presented for comparison. The solid line represents calculated results using the Boltzmann transport model developed in Refs. [6, 28].

a function of C_B ranging from 5×10^{16} to 3×10^{19} cm^{-3}. For comparison, mobility data are also plotted for GS-MBE Si : B [5] and bulk Si : B [24]. $\mu_c(C_B)$ for both Si and $Si_{0.95}Ge_{0.05}$ decreases with increasing C_B primarily due to Coulomb scattering from ionized acceptors. However, the alloy films, even though they contain only 5 at% Ge, exhibit mobilities which are significantly higher than those of pure Si over the entire B concentration range. Previously published CVD results, obtained from $Si_{0.95}Ge_{0.05}$: B layers grown over the same temperature range using SiH_2Cl_2, GeH_4, and B_2H_6, exhibited conductivity mobilities ranging from 80 cm^2 V^{-1} s^{-1} with $C_B = 3 \times 10^{18}$ to 55 cm^2 V^{-1} s^{-1} with $C_B = 3 \times 10^{19}$ cm^{-3} [25]. $\mu_c(C_B)$ in the present experiments varies from 102 to 60 cm^2 V^{-1} s^{-1} over the same B concentration range.

In order to provide an additional measure of comparison for the transport properties of fully-strained B-doped GS-MBE $Si_{0.95}Ge_{0.05}$ films, theoretical mobilities were calculated as a function of x with $C_B = 2 \times 10^{18}$ cm^{-3} using the model developed by Manku and coworkers [6]. The calculations include hole scattering contributions from acoustic phonons, nonpolar optical phonons, alloy scattering, and ionized impurity scattering. Neutral impurity and hole–hole scattering were neglected since in the former case the contribution at room temperature is minor while in the latter case, strain-induced splitting of the valence bands reduces hole degeneracy effects [6]. The calculations were carried out using a band-structure and density-of-states appropriate for fully strained $Si_{0.95}Ge_{0.05}$ on Si(0 0 1) [26, 27]. Lattice mobility terms were obtained based upon first-order perturbation solutions of the low-field Boltzmann transport equation [28].

Calculated in-plane mobilities as a function of C_B are plotted in Fig. 8 for comparison with the experimental results. Considering both the assumptions inherent in the model and the uncertainties in the measurements, the agreement between the GS-MBE results and the calculated data is quite good. Alloy scattering in $Si_{1-x}Ge_x$ acts to reduce carrier mobilities compared to Si. Thus, the measured results in Fig. 8 showing higher μ_c values for $Si_{0.95}Ge_{0.05}$ indicate that the loss due to alloy scattering is more than overcome by other effects associated with alloying and the presence of in-plane compressive strain. The primary factor increasing μ_c in these dilute alloys is a decrease in the hole effective mass resulting from changes in valence band curvature.

Hall mobilities μ_H in B-doped $Si_{0.95}Ge_{0.05}$ alloys were also measured and found to be less than values obtained for Si : B and significantly less than μ_c. With $C_B = 2 \times 10^{18}$ cm^{-3}, μ_H = 57 cm^2 V^{-1} s^{-1} for $Si_{0.95}Ge_{0.05}$ compared to 64 cm^2 V^{-1} s^{-1} for Si. The corresponding conductivity mobilities for the alloy and Si samples are μ_c = 110 and 86 cm^2 V^{-1} s^{-1}, respectively. Thus, the Hall scattering factor $\gamma = \mu_H/\mu_c$ decreases from 0.75 for Si with $C_B = 2 \times 10^{18}$ cm^{-3}, in good agreement with the accepted value for bulk Si [29], to 0.52 for $Si_{0.95}Ge_{0.05}$. The decrease in γ for $Si_{1-x}Ge_x$ is consistent with previous MBE [25, 30] and CVD [25] results. Finally, we find for $Si_{0.95}Ge_{0.05}$: B

that γ is approximately constant as a function of C_B with a slight tendency to decrease with increasing B concentration, following the behavior of bulk p-type Si [29]. Overall, γ for $Si_{0.95}Ge_{0.05}:B$ is $\simeq 0.49 \pm 0.05$.

Physically, γ is a parameter which accounts for the fact that the standard free-electron gas model used to obtain μ_H from measurements of the Hall coefficient assumes that all particles have the same velocity rather than a distribution of velocities [31]. Thus, the Hall mobility corresponds to the conductivity mobility of only those carriers whose velocity is equal to the average velocity of the distribution. Based upon a solution to the Boltzmann transport equation within the momentum relaxation time approximation, γ can be expressed as $\langle\tau^2\rangle/\langle\tau\rangle^2$, where the brackets signify averages over the equilibrium hole distribution function f. The averaging is required in order to account for the distribution of particle velocities [32] and f, the number of particles per quantum state in a given region of space, is a function of both real-space and reciprocal-space coordinates. Thus, the decrease in γ upon alloying is due to a complex combination of changes in the energy-dependence of operative hole scattering mechanisms and the amount of valence band warpage.

4. Conclusions

Fully strained heteroepitaxial B-doped $Si_{0.95}Ge_{0.05}$ alloys were grown on Si(0 0 1) by GS-MBE from Si_2H_6, Ge_2H_6, and B_2H_6 in the high-temperature (600–700°C) range of the surface-reaction-limited regime. B_2H_6 fluxes were varied from 6×10^{12} to 2×10^{15} $cm^{-2}\,s^{-1}$ to provide B concentrations between 5×10^{16} to 3×10^{19} cm^{-3}. SIMS profiles obtained from the modulation-doped and single-layer samples showed no indication of B surface segregation. B_2H_6 reactive sticking probabilities were estimated, based upon a simple extrapolation of previous models derived for Si_2H_6 and Ge_2H_6 surface reaction kinetics [1, 2], to range from 3.3×10^{-4} at $T_s = 600$°C to 8.2×10^{-4} at 700°C.

Room-temperature conductivity mobilities in these B-doped $Si_{0.95}Ge_{0.05}$ alloys were up to a factor of two larger than corresponding values for Si. μ_c varied from 410 $cm^2\,V^{-1}\,s^{-1}$ with $C_B = 5\times10^{16}$ cm^{-3} to 60 $cm^2\,V^{-1}\,s^{-1}$ with $C_B = 3\times10^{19}$ cm^{-3}. Measured μ_c values were in good agreement with calculated values based upon a Boltzmann transport model developed by Manku and coworkers [6, 28]. The Hall scattering factor γ for B-doped $Si_{0.95}Ge_{0.05}$ was found to be 0.49 ± 0.05.

Acknowledgements

The authors gratefully acknowledge the financial support of the Office of Naval Research, through contract number N00014-81-K-0568 administered by Drs. Al Goodman and Larry Cooper, the Semiconductor Research Corporation, and the Materials Science Division of the US Department of Energy under contract number DEAC0276ER01198 during the course of this research. We also thank N.-E. Lee for the TEM analyses.

References

[1] T.R. Bramblett, Q. Lu, T. Karasawa, M.-A. Hasan, S.K. Jo and J.E. Greene, J. Appl. Phys. 76 (1994) 1884.
[2] T.R. Bramblett, Q. Lu, N.-E. Lee, N. Taylor, M.-A. Hasan and J.E. Greene, J. Appl. Phys. 77 (1995) 1504.
[3] Q. Lu, M.R. Sardela Jr., T.R. Bramblett and J.E. Greene, J. Appl. Phys. 80 (1996) 4458.
[4] K. Sinniah, M.G. Sherman, L.B. Lewis, W.H. Weinberg, J.T. Yates and K.C. Jandas, J. Chem. Phys. 92 (1990) 5700.
[5] Q. Lu, T.R. Bramblett, N.-E. Lee, M.-A. Hasan, T. Karasawa and J.E. Greene, J. Appl. Phys. 77 (1995) 3067.
[6] T. Manku, J.M. McGregor, A. Nathan, D.J. Roulston, J.-P. Noël and D.C. Houghton, IEEE Trans. Electron. Dev. 40 (1993) 1990.
[7] X.-J. Zhang, G. Xue, A. Agarwal, R. Tsu, M.-A. Hasan, J.E. Greene and A. Rockett, J. Vac. Sci. Technol. A 11 (1993) 2553.
[8] R.L. Dolittle, Nucl. Instrum. Methods B 15 (1985) 344.
[9] L.J. van der Pauw, Phillips Res. Rep. 13 (1958) 1.
[10] T.R. Bramblett, Q. Lu, M.-A. Hasan, S.K. Jo and J.E. Greene, unpublished.
[11] B-M.H. Ning and J.E. Crowell, Surf. Sci. 295 (1993) 79.
[12] B.S. Meyerson, K.J. Uram and F.K. LeGoues, Appl. Phys. Lett. 53 (1988) 2555.
[13] S.-M. Jang and R. Reif, Appl. Phys. Lett. 59 (1991) 3162.
[14] D.J. Robbins, J.L. Glasper, A.G. Gullis and W.Y. Leong, J. Appl. Phys. 69 (1991) 3729.

[15] M.A.G. Halliwell, M.H. Lyons, S.T. Davey, M. Hockley, C.G. Tuppen and C.J. Gibbings, Semicond. Sci. Technol. 4 (1989) 10.
[16] D. Taupin, Bull. Soc. Franc. Miner. Crist. 87 (1964) 469.
[17] S. Takagi, J. Phys. Soc. Jpn. 26 (1969) 1239.
[18] P. Fewster, Semicond. Sci. Technol. 8 (1993) 1915.
[19] P. Fewster, J. Appl. Crystallogr. 22 (1989) 64.
[20] J. Lee, W.E. Mayo and T. Tsakalakos, J. Electron. Mater. 21 (1991) 867.
[21] M.L. Yu, J. Vitkavage and B.S. Meyerson, J. Appl. Phys. 59 (1986) 4032.
[22] F.J. Morin and J.P. Maita, Phys. Rev. 96 (1954) 28.
[23] S.K. Chun and K.L. Wang, IEEE Trans. Electron. Dev. 39 (1992) 2153.
[24] D.M. Caughy and R.E. Thomas, Proc. IEEE 55 (1967) 2192.
[25] T.K. Carns, S.K. Chun, M.O. Tanner, K.L. Wang, T.I. Kamins, J.E. Turner, D.Y.C. Lie, M.-A. Nicolet and R.G. Wilson, IEEE Trans. Electron. Dev. 41 (1994) 1273.
[26] R. People and J.C. Bean, Phys. Rev. B 32 (1985) 1405.
[27] T. Manku and A. Nathan, Phys. Rev. B 43 (1991) 12634.
[28] T. Manku and A. Nathan, IEEE Electron. Dev. Lett. 12 (1991) 704.
[29] J.F. Lin, S.S. Li, L.C. Linares and K.W. Teng, Solid-State Electron. 24 (1981) 827.
[30] J.M. McGregor, T. Manku, J.-P. Noël, D.J. Roulston, A. Nathan and D.C. Houghton, J. Electron. Mater. 22 (1993) 319.
[31] J.P. Mckelvey, Solid-State and Semiconductor Physics (Harper & Row, New York, 1966) p. 289.
[32] C.M. Wolfe, N. Holonyak Jr. and G.E. Stillman, Physical Properties of Semiconductors (Prentice-Hall, Englewood Cliffs, NJ, 1989) p. 169.